Materials Research Express

PAPER • **OPEN ACCESS**

Zeolite/ZnO composites based on a Cuban natural clinoptilolite and preliminary evaluation in methylene blue adsorption

Materials Research Express

PAPER

Zeolite/ZnO composites based on a Cuban natural clinoptilolite and preliminary evaluation in methylene blue adsorption

Yailen Costa-Marrero[1], **Marcelo B de Andrade**[2], **Javier Ellena**[2], **Julio Duque-Rodríguez**[3], **Tania Farías**[3,4] **and Giselle Autié-Castro**[3,4]

[1] Universidad de las Ciencias Informáticas, km 2½ Autopista La Habana - San Antonio de los Baños, La Habana, Cuba
[2] Instituto de Física de São Carlos, Universidade de São Paulo, Av. Trab. São-Carlense, 400 - Parque Arnold Schimidt, São Carlos - SP, 13566-590, Brazil
[3] Institute of Materials Science and Technology, University of Havana, Zapata y G, S/N, Plaza de la Revolución, CP 10400, Havana, Cuba
[4] Authors to whom any correspondence should be addressed.

E-mail: tania@imre.uh.cu **and** gautie@imre.uh.cu

Keywords: composite, clinoptilolite, ZnO nanoparticles, mechanosynthesis, '*in situ*' synthesis

OPEN ACCESS

RECEIVED
11 October 2019

REVISED
7 January 2020

ACCEPTED FOR PUBLICATION
10 January 2020

PUBLISHED
20 January 2020

Abstract

Two composites based on a Zn^{2+} exchanged natural clinoptilolite and ZnO nanoparticles were obtained by mechanosynthesis and '*in situ*' methods. Characterization of resulting materials was carried out using XRD, Raman spectroscopy, TGA, FE-SEM and N_2 adsorption. XRD results showed that no significant changes in the crystalline structure of the zeolite took place due to the performed treatments. Thermogravimetric behaviour indicated a high thermal stability for all samples. Raman spectra exhibited the characteristic bands for clinoptilolite zeolite and ZnO reported in the literature and the RRUFF database. Morphology changes were observed between natural and exchanged clinoptilolite and the '*in situ*' obtained composite. Textural analysis showed a decrease in surface area of '*in situ*' composite compared with the exchanged zeolites, related to the partial nanoparticle deposition in the pore entrances. The adsorption studies of methylene blue in the zeolitic samples and composites showed that all evaluated materials were able to absorb the dye from aqueous solutions.

1. Introduction

Composite materials can be defined as two or more different materials that when combined result in a material with properties that exceed those of the individual components [1–3]. A nanocomposite is a composite or multiphase material where one of the phases has one, two or three dimensions less than 100 nm [4]. This definition includes porous media, colloids, gels and copolymers; but it is more common to combine a solid that acts as a matrix and a phase (or more) nanometer scattered in the matrix. The complex interaction of the nanostructured heterogeneous phases conduces to interesting properties in the nanocomposites [5]. Nanocomposites are used in many applications, such as in biomedicine, electronics and environmental remediation. Therefore, the study of nanocomposite materials is a fast-growing area of research [4, 6, 7].

Zeolites are the most important group of hydrated aluminosilicates which are characterized by a complex three-dimensional framework of linked tetrahedral, leading to the presence of open cavities in the form of channels and cages, which are usually occupied by H_2O molecules and extra-framework cations. Each tetrahedral consists of four oxygen atoms surrounding a tetrahedral atom (T) usually Si and Al. The peculiar structure of the zeolites gives these materials excellent properties such as ion exchangers, adsorbents and catalysts, which is why they have been used in a wide field of applications [8].

Nanoparticles are particles that exist on a nanometer scale (i.e., below 100 nm in at least one dimension). They can possess physical properties such as uniformity, conductance or special optical properties that make them desirable in materials science and biology. ZnO nanoparticles (ZnO NPs) are been widely explored due to their antifungal, catalyst and adsorbent properties [9–11]. Recently, ZnO NPs have been evaluated in CH_4 and CO_2 separation and adsorption [12].

Methylene Blue (MB) is a dye usually used by chemical, printing and textile industries, which causes water contamination hazardous to human and animal health [13]. Therefore, its recovery from industrial wastewater by using different methods is much studied. Traditional treatment methods have been used to remove organic pollutants such as: adsorption on activated carbons and zeolites, as well as, disinfection by-products [14–16]. MB adsorption have been evaluated by using clays minerals, zeolites, red mud, graphene, among others materials [17–19]. The photodegradation of methylene blue has been also very studied [20–22]. It has been reported the use of different semiconductor metal oxides like TiO_2, CuO and ZnO, either alone or supported in porous materials for such purpose [23–26].

In this paper, mechanosynthesis and '*in situ*' methods are used for obtaining composites based on Zn^{2+} exchanged natural clinoptilolite and ZnO nanoparticles. Mechanosynthesis is a mechanical-assisted process where chemical changes are achieved by the action of grinding (or milling), without the addition of solvents, therefore is environmental friendly [27]. In our case, the mechanosyntesis was carried out by grinding together the zeolite with previously synthesized ZnO nanoparticles. In the '*in situ*' method the nanoparticles are synthesized directly over the zeolitic matrix. Structural characteristics, topology and porosity of the obtained materials are discussed and compared with parent clinoptilolite in order to evaluate their future applications in catalysis, gases capture and residual wastewater treatment. In this sense, a preliminary study of MB adsorption from aqueous solutions was also carried out.

2. Experimental

2.1. Reagents

Sodium chloride (NaCl, ACS reagent, ⩾99.0%), zinc nitrate hexahydrated ($Zn(NO_3)_2$ x $6H_2O$, reagent grade, 98%), zinc acetate dihydrated ($Zn(O_2CCH_3)_2$ x $2H_2O$, ACS reagent, ⩾98%), oxalic acid ($H_2C_2O_4$, ReagentPlus®, ⩾99%) and sodium hydroxide (NaOH, ACS reagent, ⩾97%) were purchased from Sigma-Aldrich and were used without further purification. Methylene blue ($C_{16}H_{18}ClN_3S$ x nH_2O, n = 2–3, Reag. Ph Eur) and ethanol (C_2H_5OH, absolute EMPLURA®) were purchased from Merck.

2.2. Pre-treatment of clinoptilolite sample

Clinoptilolite with general formula $(Na,K,Ca_{1/2})_6[Al_6Si_{30}O_{72}]$ x $24H_2O$ [28] from Tasajeras deposit, Villa Clara, Cuba, was used in this work. The zeolite was previously dry sieved using a sieve battery. The fraction of particle size between 56–71 μm was selected. Purification of natural clinoptilolite was performed by three washes steps with distilled water during 4 h at room temperature and magnetic stirring followed by three washes steps using the same procedure but at 80 °C. Subsequently, the exchange with 1 M sodium chloride (NaCl) solution was carried out at 100 °C for 8 h, using a solid/liquid ratio of 1 g/5 ml. Na^+ exchanged clinoptilolite (Na-cli) was washed several times to remove the excess of chloride and then was exchanged with 0.1 M zinc nitrate ($Zn(NO_3)_2$), similarly to the sequence previously explained. The obtained sample (Zn-cli) was washed repeatedly with distilled water to remove the nitrate ions. Finally, the sample was dried at 100 °C overnight.

2.3. Obtaining of ZnO nanoparticles

ZnO nanoparticles were synthesized by dissolving 1.0952 g of zinc acetate $Zn(O_2CCH_3)_2$ in 30 ml of ethanol at 60 °C. Subsequently, 1.2600 g of oxalic acid ($H_2C_2O_4$) were dissolved in 20 ml of ethanol at 50 °C. The oxalic acid solution was added slowly under stirring to the hot ethanolic solution of zinc acetate. The white gel formed was dried at 80 °C during 20 h. The xerogel was calcined at 600 °C during 2 h to obtain the ZnO nanoparticles [12].

2.4. Obtaining of composites

For mechanosynthesis about 500 mg of Zn-cli and 100 mg of ZnO nanoparticles (5:1 ratio) were grinded in an agate mortar with an agate pestle at room temperature for 30 min. The obtained composite was labelled as Zn-cli/ZnO NPs (mechanosynthesis). For '*in situ*' synthesis about 1 gram of Zn-cli was dispersed in 20 ml of distilled water at room temperature under stirring. Sodium hydroxide (NaOH) 1 M solution was added drop by drop until the dispersion reach a pH = 12 and then it was leaved to react for 2 h at room temperature. After this time the suspension was filtered and the solid was dried at 60 °C overnight. Finally, the sample was calcinated at 300 °C during 2 h. The obtained composite was denoted as Zn-cli/ZnO NPs ('*in situ*').

2.5. Characterization

X-ray powder diffraction patterns of the samples were taken on a Rigaku Ultima IV diffractometer, using nickel-filtered CuKα x-ray source at a scanning rate of 0.0200° seg^{-1} over the range between 5.0° to 80.0°. The powder diffraction patterns were indexed with impurity peaks using the program DICVOL04 [29] to a monoclinic lattice and M20 = 34.7 [30]. A Le Bail fit [31] was carried out using the program FullProf [32] and confirmed the lattice

found. The Le Bail agreement factors for Na-cli were: Bragg R-factor = 1.09, Rf-factor = 0.818 and Chi^2 = 3.17 and for Zn-cli were: Bragg R-factor = 13.7, Rf-factor = 5.44 and Chi^2 = 3.92. ZnO NPs XRD was compared with the zinc oxide (ZnO) ICCD PDF 36-1451 [33].

Raman spectra were collected from a randomly oriented crystal on a LabRAM HR Evolution microRaman spectrometer system, using a 532 and 633 nm laser excitation and a spectral resolution of 1 cm^{-1} with a thermoelectric cooled CCD detector.

Thermogravimetric analysis curves were obtained with a Shimadzu TGA-60 thermogravimetric analyzer (Shimadzu Inc. Kyoto, Japan), using alumina pan, flowing nitrogen at 150 ml min^{-1}, and a heating rate of 5 °C min^{-1} from room temperature to 600 °C. Measures were collected and processed with TA60 software associated to the analyzer. About 10 mg of each samples in powder form were used as initial mass for the thermogravimetric analysis.

Morphology study of the starting compounds as well as the resulting composites was carried out using a ZEISS Sigma model Field Emission Scanning Electron Microscope (FE-SEM). Samples were recovered with platinum. The determination of the particle size for the ZnO nanoparticles, was carried out using ImageJ version 1.38× software. The particle size data was fitted assuming a normal probability density function. The adjusted was based on a count of 150 individual nanoparticles.

N_2 adsorption-desorption isotherms were collected at 77 K as a function of relative pressure P/P_0 over the range of 0.01–0.99 by using a Micromeritics ASAP 2020 volumetric adsorption analyzer. Samples were outgassed at 250 °C for 12 h under vacuum prior to each measurement. Specific surface areas (S_{BET}) of all materials were calculated according to the Brunauer-Emmett-Teller (BET) method using adsorption data in the relative pressure P/P_0 range of 0.05–0.2 [34]. The total pore volumes (V_t) were estimated from the amount adsorbed at the relative pressure of 0.98. The pore size distribution (PSD) was calculated by using the improved Barrett-Joyner-Halenda (BJH) model evaluated from the desorption branch [35].

2.6. Preliminary study of methylene blue adsorption

Methylene Blue (MB) adsorption was studied by mixing 250 mg of Na-cli, Zn-cli, Zn-cli/ZnO NPs (mechanosynthesis) or Zn-cli/ZnO NPs ('*in situ*') and 80 ml of a MB solution of concentration 2 mg l^{-1}, and keeping in contact for 45 min. The system was covered with aluminum foil to avoid light incidence. Aliquots of about 5 ml were collected at: 5, 10, 15, 20, 30 and 45 min, to determine MB concentration by UV-Vis spectroscopy. The measurements were performed using an UV-Vis 1800 Spectrophotometer from Shimadzu at a wavelength of 700 nm. After 45 min the supernatants were decanted and the solid was dried at 40 °C (to avoid thermal decomposition of the dye) and analysed by Raman spectroscopy.

3. Results and discussion

3.1. Characterization of the starting materials and the composites

X-rays diffraction (XRD) patterns of Na-cli, Zn-cli, ZnO NPs and composites Zn-cli/ZnO NPs obtained by mechanosynthesis and '*in situ*' methods are shown in figure 1 while table 1 resumes the cell parameters for the starting materials.

Clinoptilolite (which belong to the heulandite framework type) crystallizes in monoclinic system [28]. The monoclinic crystalline system was confirmed by the Le Bail method for Na-cli, Zn-cli and the obtained composites in agreement with previous reports [28]. Therefore, there were no changes in the crystalline structure due to the incorporation of the nanoparticles by both methods. As the zeolite used is a material of natural origin, the presence of other phases, such as mordenite and quartz, can be observed in the diffractograms of the parent zeolites (Na-cli and Zn-cli). The diffraction maxima of contaminant quartz phase (which should be unaffected by the purification, ion exchange and nanoparticles inclusion) were also observed in the patterns of the composites. In addition, the relative intensity of some diffraction maxima changes from Na-cli to Zn-cli, which could be interpreted as a consequence of the ion exchange [36, 37].

The diffraction maxima of ZnO NPs were assigned to the characteristic planes of the hexagonal wurzite structure which crystallizes in the $P6_3mc$ space group, in agreement with the crystal structure and the lattice parameters of zinc oxide (ZnO) [33]. Narrow diffraction peaks were obtained, suggesting good crystallinity. The ZnO NPs diffraction maxima are also observed in composite obtained by mechanosynthesis method, as was expected since the nanoparticles are in a 20 weight percent in the composite. However, ZnO NPs diffraction maxima were not observed in the composite obtained by '*in situ*' method. This could be probably due to the small amount of nanoparticles obtained by this method, together with the small particle size.

The Raman spectra of the studied materials are shown in figure 2. They were compared with the spectra reported in the RRUFF database (http://rruff.info/), finding a good match for clinoptilolite zeolite. In general,

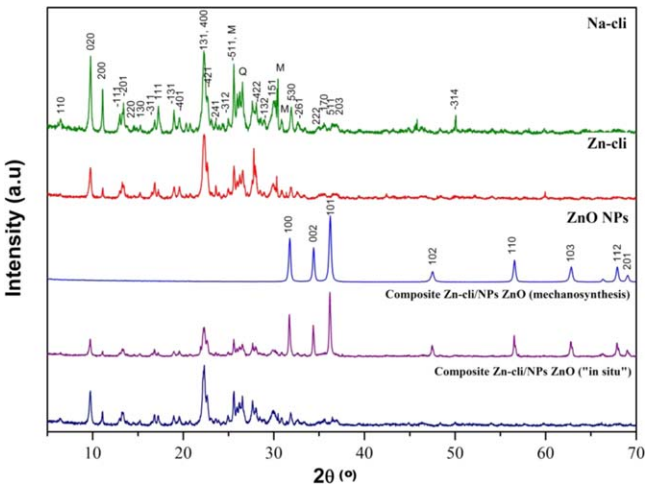

Figure 1. XRD patterns of starting materials (Na-cli, Zn-cli and ZnO NPs) and resulting composites obtained by mechanosynthesis and '*in situ*' methods. The *hkl* index corresponding to clinoptilolite and ZnO are reported in the figure, while the peaks corresponding to mordenite and quartz phases are labelled as M and Q, respectively.

Table 1. Cell parameters of the starting materials obtained by Le Bail fit.

Sample	*a* (Å)	*b* (Å)	*c* (Å)	*β* (°)
Na-cli	17.721(1)	18.053(3)	7.394(5)	116.49(7)
Zn-cli	15.228(4)	18.471(4)	14.771(1)	113.86(1)
ZnO NPs	3.24170(8)	5.18760(8)		

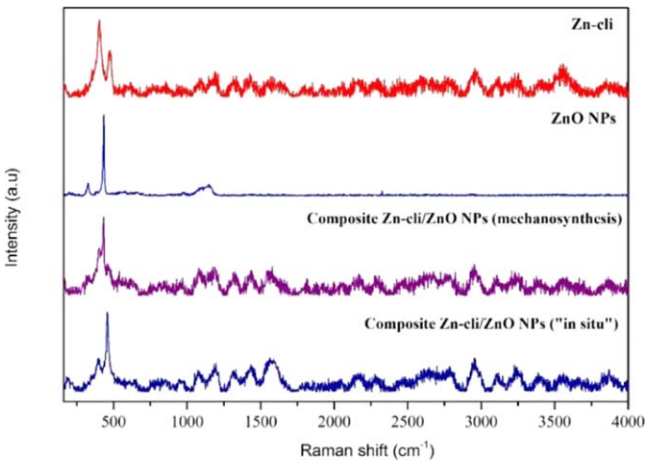

Figure 2. Raman spectrum of starting materials (Zn-cli, ZnO NPs) and resulting composites obtained by mechanosynthesis and '*in situ*' methods.

the strongest characteristic bands of the zeolites appear between 300–600 cm^{-1} of the spectral range and are attributed to the movement of the oxygen atom in the plane perpendicular to the T-O-T bonds [38].

Table 2 shows the Raman bands of the studied samples. The spectrum of the Zn-cli shows the most intense bands at 403 and 472 cm^{-1} that are assigned to the vibrations $\nu_2(E)$ and $\nu_4(F_2)$ of the tetrahedral SiO_4 units [38]. In addition, bands in the characteristic region of water stretching vibrations (2800–3800 cm^{-1}), due to water molecules in the sample cavities, are clearly observed. The spectrum of ZnO NPs shows the most intense band at 433 and a band at 327cm^{-1} corresponding to the E_2(high) and E_2(high)-E_2(low) of the ZnO, respectively [39]. The incorporation of ZnO nanoparticles in the composites obtained by the '*in situ*' method can be verified because the Raman spectra of both composites not only exhibited the major bands previously assigned to the Zn-cli but also the bands at 432 and 457 cm^{-1} related to the ZnO NPs. In addition, a slight shift in the ZnO band

Table 2. Tentative assignment of major Raman bands observed in the evaluated samples.

Raman shift (cm^{-1})				
Zn-cli	ZnO NPs	Zn-cli/ZnO NPs (mechanosynthesis)	Zn-cli/ZnO NPs (‘***in situ***’)	Assignment
—	327	—	—	E_2(high)-E_2(low)
403	—	402	397	$\nu_2(E)$ SiO_4
—	433	432	457	E_2(high) ZnO
472	—	—	—	$\nu_4(F_2)$ SiO_4
2800–3800	—	2800–3800	2800–3800	H_2O stretching

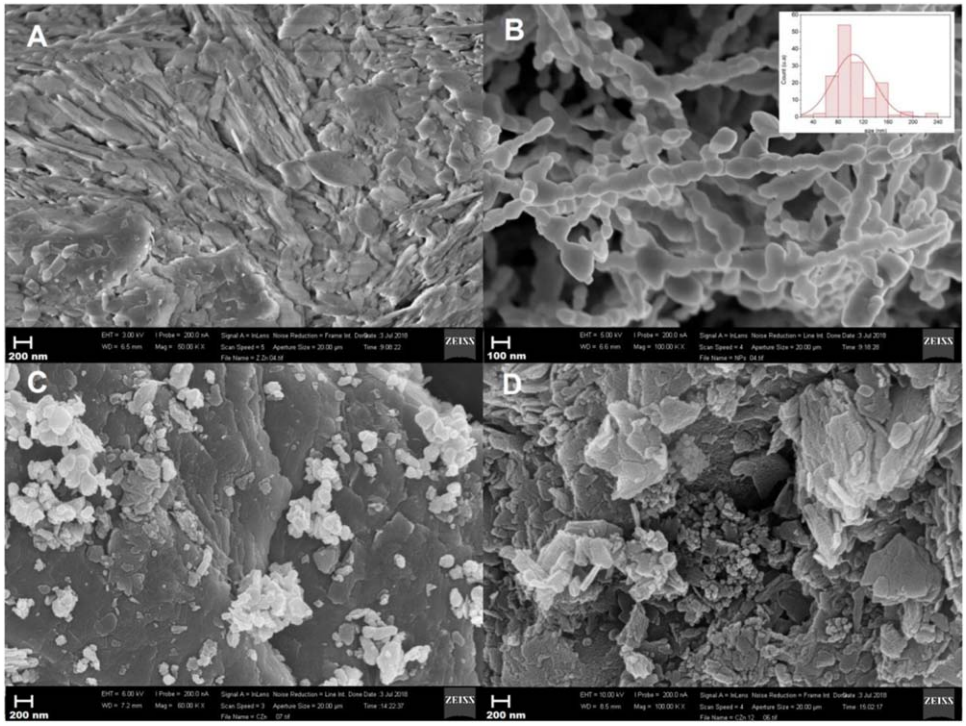

Figure 3. FE-SEM images of: Zn-cli (A), ZnO NPs (B), Zn-cli/ZnO NPs (mechanosynthesis) (C) and Zn-cli/ZnO NPs (‘*in situ*’) (D). The inserted graph shows the histogram of particle size distribution of ZnO NPs.

in the spectrum of Zn-cli/ZnO NPs ‘*in situ*’ is observed, which could be ascribed to the sample calcination after the basic treatment.

Figure 3 shows the FE-SEM images of the starting materials and the obtained composites. Zn-cli exhibits a zeolite characteristic irregular surface fine-graining material of lamellar texture. ZnO NPs presents a quite uniform shape with particle size in the range of 60–180 nm and an average diameter of 90 nm. As can be seen, the nanoparticles tend to organize forming chains. In the composite obtained by mechanosynthesis the chain structure of ZnO NPs is not observed, instead the ZnO NPs are incorporated as agglomerates distributed heterogeneously on the zeolitic surface, which is derived from the grinding process. The ZnO NPs are not clearly observed in the FE-SEM image of the composite obtained by ‘*in situ*’ method (figure 3(D)). However, their presence was confirmed by Raman spectroscopy, as was previously discussed.

Figure 4 shows the thermogravimetric curves of Na-cli, Zn-cli, ZnO NPs and the two composites. TG analysis demonstrated a high thermal stability for all studied materials. In the case of Na-cli the mass loss from room temperature to about 80 °C is assigned to the loss of physisorbed water. The continuous mass loss up to about 350 °C is due to the gradual release of the water coordinated to the exchangeable cations. For Zn-cli sample the percent of mass loss is greater than for Na-cli and both peaks appear at higher temperature. This behaviour is related to the cation present in each case and the amount of water coordinated to them. The DTG curve of ZnO NPs shows a mass loss of approximately 5% between 30 °C–150 °C with a peak at 50 °C that could be ascribed to the loss of physisorbed water. The DTG curves of the composites showed marked differences. The curve of the composite obtained by mechanosynthesis is very similar to that of Zn-cli sample, while the curve of the composite obtained by ‘*in situ*’ method is very similar to that of Na-cli sample. This could be due to the

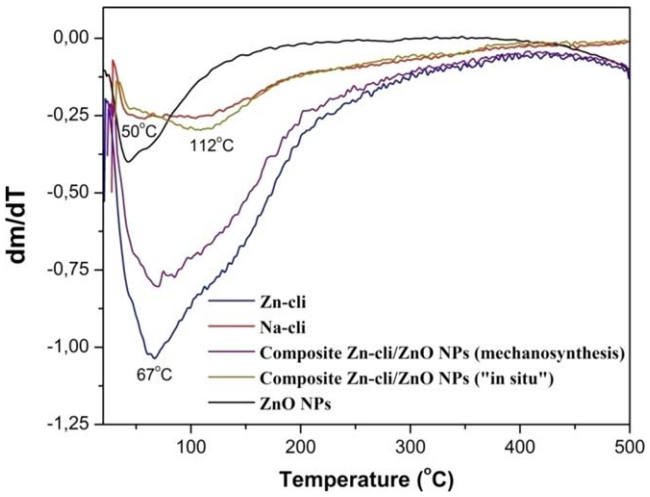

Figure 4. Thermogravimetric curves of the studied samples.

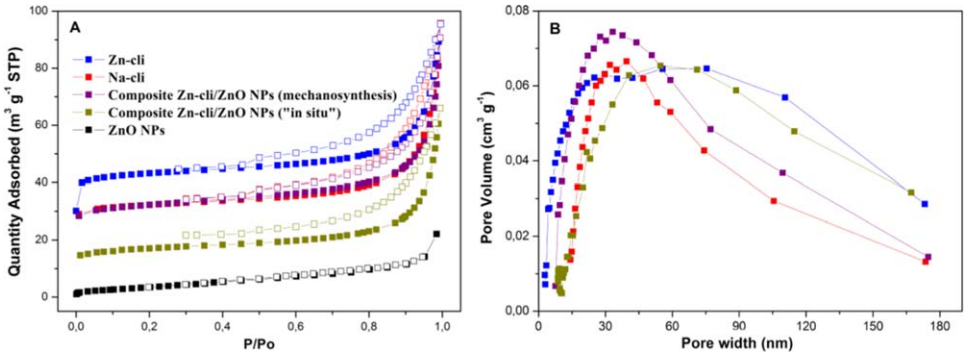

Figure 5. N_2 adsorption isotherms at 77 K (A), where filled symbols correspond to adsorption branch and empty symbols correspond to desorption branch, and porous size distribution of the studied samples (B).

Table 3. Textural properties of the evaluated samples obtained by N_2 adsorption-desorption at 77 K.

Sample	S_{BET}(m^2g^{-1})	V_{mic}(cm^3g^{-1})	V_t(cm^3g^{-1})	BJH average pore diameter(nm)
Na-cli	111	0.04	0.14	15.67
Zn-cli	149	0.06	0.14	13.12
ZnO NPs	11	—	0.03	—
Zn-cli/ZnO NPs (mechanosynthesis)	112	0.04	0.13	15.84
Zn-cli/ZnO NPs (‘*in situ*’)	60	0.02	0.09	15.87

S_{BET} = obtained from adsorption data at $0.05 < P/P_0 < 0.2$,
V_{mic} = calculated by t-plot method,
V_t = amount of N_2 adsorbed at the $P/P_0 = 0.99$

partial replacement of Zn^{2+} by Na^+ cations during the treatment with NaOH in the ‘*in situ*’ composite synthesis. In addition, the partial blockages of the zeolite channel system by the ZnO nanoparticles takes place, which avoid the release of water, as will be seen later.

Figure 5 shows the N_2 adsorption isotherms at 77 K and the porous size distribution (PSD) of Na-cli, Zn-cli, ZnO NPs and the two composites, while textural properties are summarized in table 3.

The N_2 adsorption-desorption isotherms of the zeolites and the composites samples (figure 5(A)) were of type IV with hysteresis loop of type H3, characteristics of capillary condensation in parallel plate-shaped pores according to the IUPAC classification [40], while ZnO NPs exhibits a type II isotherm. The results show an increase of the surface area from Na-cli to Zn-cli, behaviour that is common when a replace of a monovalent cation by a divalent one is carried out. When the Zn^{2+} exchange process occurs, one Zn^{2+} cation occupies the place of two Na^+ cations which leads to a surface area increment. The composites show a surface area lower than

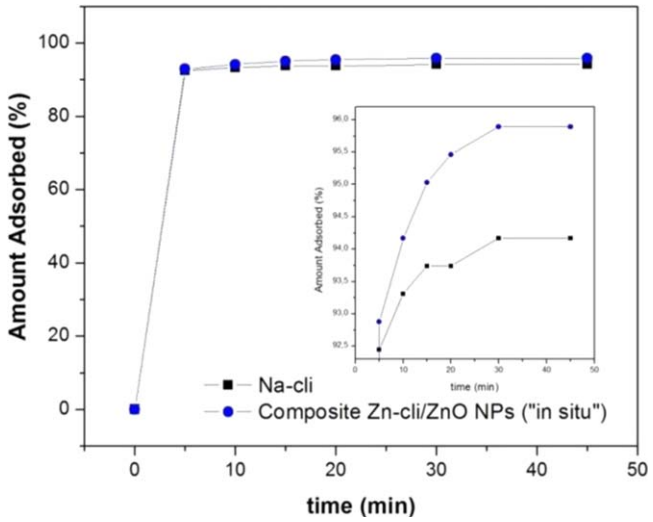

Figure 6. Amount of MB adsorbed versus time for Na-cli and composite Zn-cli/ZnO NPs ('*in situ*') samples.

that of the parent Zn-cli, and this decrease is higher for the '*in situ*' composite (see table 3). This result indicates that the addition of ZnO NPs into the zeolitic matrix by grinding is a not-uniform process in which nanoparticles tend to deposit at the zeolitic surface. This process occasionally blocks the pore entrances while in the '*in situ*' method the nanoparticles are formed preferentially at the entrance of the pores and channels of the clinoptilolite making difficult the N_2 diffusion inside de pores. These results fit with the obtained values of total and micropore volume (V_t and V_{mic}) reported in table 3, where a slight decrease in V_{mic} for Zn-cli/ZnO NPs ('*in situ*') sample is observed. This result is also coherent with those obtained by TG analysis, where the '*in situ*' composite shows a lower loss of water.

Clinoptilolite owns free dimensions channels of approximately: $a \approx 7.5 \times 3.1$ Å, $b \approx 4.6 \times 3.6$ Å and $c \approx 4.7 \times 2.8$ Å [28] which is known as primary porosity (microporosity) and is the result of their open framework structure. It is known that zeolites also present a secondary porosity that is usually represented by a system of meso-and macropores [41], and is related with the inter particle space due to the specific grain packing of zeolite and other minerals in the zeolitic rocks, as well as, cleavage degree of zeolite grains.

The mesopores are transport channels that can improve the efficiency of zeolitic materials as catalysts and adsorbents, since they favour the diffusion and adsorption of large molecules. In addition, some technological properties, which cannot be explained by adsorption in micropores, could be conditioned by secondary porosity [42]. Figure 5(B) shows the pore size distribution (PSD) of the zeolitic samples. The existence of secondary porosity was confirmed by this analysis, which was not apparently affected by the ZnO nanoparticle incorporation using both methods. In addition, the majority presence of mesopores between 3–30 nm was observed.

3.2. Methylene blue adsorption

When MB is put in contact with the clinoptilolite and the composite samples, a rapid discoloration of the solution is observed. For Zn-cli and composite Zn-cli/ZnO NPs (mechanosynthesis) samples, was not possible to detect MB by UV-Vis in the remaining solution after the first 5 min of interaction, indicating a very fast adsorption of the dye. For Na-cli and composite Zn-cli/ZnO NPs ('*in situ*') samples the amount of MB adsorbed versus time is shown in figure 6. As can be seen, the adsorption is also fast for these samples, reaching the equilibrium at 30 min of interaction (see inset). The maximum amount adsorbed is greater for the composite demonstrating the role of Zn and/or ZnO NPs in the adsorption process.

Raman spectroscopic analysis of all the solid samples was carried out for checking the MB presence. The Raman spectra as well as the images obtained at optical microscope for evaluated samples and the MB are shown in figure 7.

The characteristic peaks of MB at 448 cm^{-1} and 501 cm^{-1} are attributed to the C−N−C skeletal deformation mode. In-plane bending mode of C−H is observed at 770 cm^{-1} and 1154 cm^{-1}, while in-plane ring deformation mode of C−H is at 1302 cm^{-1}. The two prominent peaks at around 1394 cm^{-1} and 1623 cm^{-1} are assigned to C−N symmetrical stretching and C−C ring stretching, respectively [43]. These typical Raman bands are clearly observed in all the studied samples, which are related to the MB adsorption by the solid. The images on the right of figure 7 exhibited a blue coloration that also denotes the presence of MB in the samples.

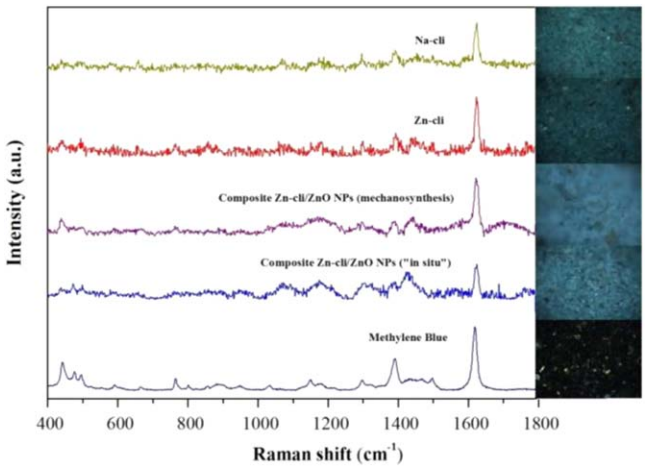

Figure 7. Raman spectra and obtained images of MB and Na-cli, Zn-cli, Zn-cli/ZnO NPs (mechanosynthesis), Zn-cli/ZnO NPs ('*in situ*') after 45 min of contact with MB solution.

The MB molecule has a rectangular shape with dimensions 17 Å × 7.6 Å × 3.25 Å. The surface area covered by one MB molecule is assumed to be approximately 130 $Å^2$ [44]. The adsorption of this molecule into the micropore system of the clinoptilolite is not possible due to size restrictions. Thus, the adsorption of MB could be ascribed to the migration of MB molecules into the meso and macroporous system corresponding to the presence of secondary porosity observed by BJH method.

4. Conclusions

Two composites were obtained from a Cuban natural clinoptilolite by mechanosynthesis and '*in situ*' via. XRD showed that the crystal system (monoclinic) did not change when clinoptilolite was exchanged with Na^+ and Zn^{2+} and when the nanoparticles were included. Raman spectra exhibited characteristic bands of zeolites and ZnO reported in the literature and the RRUFF database. Changes in morphology of composite obtained by '*in situ*' via compared with clinoptilolite's laminar morphology were observed. A high thermal stability was also exposed. N_2 adsorption experiments revealed a decrease in the surface area in the composite obtained by '*in situ*' method, which could be ascribed to the nanoparticle deposition at the entrances of the micropores. The preliminary MB adsorption studies disclosed a very fast adsorption of the dye by all the evaluated solids, especially in the case of Zn-cli and composite Zn-cli/ZnO NPs (mechanosynthesis). Thus, both composites could be attractive for applications in removing of this dye from wastewaters.

Acknowledgments

The authors are grateful to the agencies CAPES (CAPES-MES Project No. 196/13), CNPq (J.E grant #305190/2017-2). Thanks to Dr María José Fonseca Costa for the N_2 adsorption measurements.

ORCID iDs

Marcelo B de Andrade https://orcid.org/0000-0001-9137-8831
Javier Ellena https://orcid.org/0000-0002-0676-3098
Tania Farías https://orcid.org/0000-0002-0171-1790
Giselle Autié-Castro https://orcid.org/0000-00020-6315-4918

References

[1] Roeseler W G, Sarh B and Kismarton M U 2007 *16th Int. Conf. on Composite Materials* (Japan: Kyoto) pp 1–10 http://www.iccm-central.org/Proceedings/ICCM16proceedings/contents/pdf/MonA/MoAM1-01sp_roeselerw228184p.pdf
[2] Campbell F C 2010 *Structural Composite Materials* 1st edn (Ohio, United States of America: ASM International)
[3] Sai M K S 2016 *Inter. J. Latest Engine. Trends Technol.* **6** 129–35 https://www.ijltet.org/journal_details.php?id=898&j_id=2831
[4] Ajayan P M, Schadler L S and Braun P V 2003 *Nanocomposite Science and Technology* (KGaA, Weinheim: Wiley-VCH Verlag GmbH & Co.)

[5] Sahoo P K, Behera D K, Dash M P, Adhikari M C and Nayak P L 2013 *The IJES* **2** 141-48 www.theijes.com
[6] Zeng Q H, Wang D Z, Yu A B and Lu G Q 2002 *Nanotechnology* **13** 549–53
[7] Zhu Y 2003 Synthesis, characterization and corrosion performance of polyaniline-montmorillonite clay nanocomposites *Department of Chemical and Materials Engineering of the College of Engineering* University of Cincinnati pp 155
[8] Moshoeshoe M, Nadiye-Tabbiruka M S and Obuseng V 2017 *Am. J. Mater. Sci.* **7** 196–221
[9] Arciniegas-Grijalba P A, Patiño-Portela M C, Mosquera-Sánchez L P, Guerrero-Vargas J A and Rodríguez-Páez J E 2017 *Appl. Nanosci.* **7** 225–41
[10] Nagajyothi P C, Minh An T N, Sreekanth T V M, Lee J I, Joo D L and Lee K D 2013 *Mater. Lett.* **108** 160–3
[11] Khan S B, Rahman M M, Marwani H M, Asiri A M and Alamry K A 2013 *Nanoscale Res. Lett.* **8** 1–8
[12] Montejo-Mesa L A, Autié-Castro G I, Cavalcante C L, Vilarrasa-García E and Díaz-García A 2018 *Revista Cubana de Química* **30** 119–30
[13] Rafatullah M, Sulaiman O, Hashim R and Ahmad A 2010 *J. Hazard. Mater.* **177** 70–80
[14] Rasheed A, Farooq F, Rafique U, Nasreen S and Aqeel Ashraf M 2016 *Desalin. Water Treat.* **57** 145–50
[15] Wang S and Peng Y 2010 *Chem. Eng. J.* **156** 11–24
[16] Kolb C, Francis R A and VanBriesen J M 2017 *J. Environ. Sci.* **58** 191–207
[17] Hang P T and Brindley G W 1970 *Clays Clay Miner.* **18** 203–12
[18] Arias M, López E, Nuñez A, Rubinos D, Soto B, Barral M T and Díaz-Fierros F 1999 Adsorption of methylene blue by red mud, an oxide-rich byproduct of bauxite refining ed E A Berthelin *Effect of Mineral-Organic-Microorganism Interactions on Soil and Freshwather Environment* (New York: Kluwer Academic/Plenum Publishers) pp 361–5
[19] Liu H *et al* 2012 *Colloids Surfaces B: Biointerfaces* **90** 197–203
[20] Nogueira R F P and Jardim W F 1993 *J. Chem. Educ.* **70** 861–3
[21] Houas A, Lachheb H, Ksibi M, Elaloui E, Guillard C and Herrmann J M 2001 *Appl. Catalysis B* **31** 145–57
[22] Du Y and Zheng P 2014 *Korean J. Chem. Eng.* **31** 2051–6
[23] Nezamzadeh-Ejhieh A and Hushmandrad S 2010 *Appl. Catal.,* A **388** 149–59
[24] Chen W, Xiao H, Xu H, Ding T and Gu Y 2015 *Int. J. Photoenergy* **2015** ID-591428
[25] Wardhani S, Rahman M F, Purwonugroho D, Tjahjanto R T, Damayanti C A and Wulandari I O 2016 *Journal of Pure and Applied Chemistry Research* **5** 19–27
[26] Subbulekshmi N L and Subramanian E 2018 *Journal of Pharmaceutical, Chemical and Biological Sciences* **6** 85–96
[27] Cova C M and Luque R 2019 *BMC Chemical Engineering* **1** 1–12
[28] Baerlocher C, McCusker L B and Olson D H 2007 *Atlas of Zeolite Framework Types* 6th edn (Amsterdam, The Netherlands: Elsevier Science)
[29] Boultif A and Louër D 2004 *J. Appl. Crystallogr.* **37** 724–31
[30] de Wolff P M 1968 *J. Appl. Crystallogr.* **1** 108–13
[31] Le Bail A, Duroy H and Fourquet J L 1988 *Mater. Res. Bull.* **23** 447–52
[32] Rodríguez-Carvajal J *Phys. B Condens. Matter.* **192** 1993 55–69
[33] Madelung O *et al* (ed) 1999 Collaboration: Authors and editors of the volumes III/17B-22A-41B, Zinc oxide (ZnO) crystal structure, lattice parameters *Semiconductors' of Landolt-Börnstein - Group III Condensed Matter.* (Berlin, Heidelberg: Springer) pp 1–5
[34] Brunauer S, Emmett P H and Teller E 1938 *J. Am. Chem. Soc.* **60** 309–19
[35] Barrett E P, Joyner L G and Halenda P P 1951 *J. Am. Chem. Soc.* **73** 373–80
[36] Petrov O E 1995 *Natural Zeolite'93: Occurrence, Properties and Use* ed D W Ming and F A Mumpton (New York: International Committee on Natural Zeolites) pp 271–9
[37] Rodríguez-Iznaga I, Gómez A, Rodríguez-Fuentes G, Benitez-Aguilar A and Serrano-Ballan J 2002 *Micropor. Mesopor. Mater.* **53** 71–80
[38] Knops-Gerrits P P, De Vos D E, Feijen E J and Jacobs P A 1997 *Microporous Mater.* **8** 3–17
[39] Cuscó R, Alarcón-Lladó E, Ibáñez J, Artús L, Jiménez J, Wang B and Callahan M J 2007 *Phys. Rev.* B **75** 165202
[40] Sing K S W 1985 *Pure Appl. Chem.* **57** 603–19
[41] Tsitsishvili G V, Andronikashvili T G, Kirov G N and Felizova L D 1992 *Natural Zeolites* (London: Ellis Horwood Limited)
[42] Mansouri N, Rikhtegar N, Panahi H A, Atabi F and Shahraki B K 2013 *Environment Protection Engineering* **39** 139–52
[43] Naujok R R, Duevel R V and Corn R M 1993 *Langmuir* **9** 1771–4
[44] Santamarina J C, Klein K A, Wang Y H and Prencke E 2002 *Can. Geotech. J.* **39** 233–41